# Power Calculations for High-Flow CO Electric Discharge Laser Systems

Neill S. Smith* and H. A. Hassan†
*North Carolina State University, Raleigh, North Carolina*

**A self-consistent model for high-flow electric discharge CO laser systems with coincident optical and flow axes is presented. The model employed couples the kinetics of the electrons and heavy particles with the optical and fluid dynamic processes in the laser system. The resulting integrodifferential system of equations governing this multilevel system was solved by an exact numerical scheme. The effects of composition, total mass flow rate and inlet pressure and temperature on the intensities, and total power output were investigated. The results indicate that, for a given input power and $N_2$ fraction, the efficiency increases by reducing the inlet temperature and increasing the velocity and/or the fraction of CO. Moreover, transitions on the lower vibrational bands can be obtained at the expense of lower efficiencies by reducing the CO fraction.**

## Introduction

THIS study is concerned with power calculations for high-flow CO-He-$N_2$ electric discharge laser systems in which the optical axis is coincident with the flow axis. Typical of these systems is the subsonic convection-cooled laser of Kan and Whitney.[1] Such systems have superior power output capability over similar slow-flow wall-cooled systems because convection cooling limits the temperature rise experienced by the gas mixture.

A number of available analyses of CO EDL (electric discharge laser) systems are for pulsed lasers[2-6] or for slow flow[7-9] lasers, which employ the steady-state approximation, i.e., where all gradients are assumed negligible. These analyses assume appropriate values for the gas and electron temperatures and the electron number density. The end effect of such assumptions is that important phenomena resulting from the coupling of electrons and heavy particles' kinetics and fluid dynamic processes are ignored. Recently, however, several investigators have presented self-consistent analyses for both supersonic[10-15] and subsonic[12,14-17] convective CO electric discharge lasers. Some of these analyses[10-15] dealt with transverse E-beam sustained discharges and transverse optical axes; others[16,17] considered geometries in which the optical axis is coincident with the flow axis. It should be noted that Hall and Eckbreth[15] have attempted to model the experiment of Kan and Whitney. However, they assumed a transverse optical axis, even though the optical axis in the experiment is coincident with the flow axis. In their initial investigation of high-flow CO EDL's with coincident optical and flow axes, Smith et al.[16] examined the effects of composition, current density, and temperature on the maximum average small signal gain coefficients under the assumption of a Maxwellian electron distribution function. In a latter work,[17] they employed an electron distribution function obtained from the solution of the electron Boltzmann equation to study the effects of composition and temperature on the maximum average small signal gain coefficients.

The present work extends the previous investigations of Smith et al.[16,17] to include laser power generation. For the flow rates under consideration, convective cooling and axial variations dominate the flow processes; therefore, wall effects are neglected, and a one-dimensional analysis is used. Because the gain coefficients and intensities vary with position along the optical (flow) axis, the procedure generally used to calculate the intensities in slow flow and transverse laser systems cannot be employed, and a new approach is developed to calculate the output power for this class of high-flow laser systems. The excitation and relaxation processes and the axial variations of pressure, temperature, velocity, number densities of species, and intensities of the lasing transitions are treated simultaneously within the optical cavity. The various parameters that depend on the electrons are calculated from the electron distribution function, which is obtained from the solution of the electron Boltzmann equation. For given inlet conditions, tube dimensions, and current density (or power) the model yields the axial variations of the gas and electron temperatures, velocity, pressure, number densities of the various species, and intensities of the lasing transitions along with the power output from each transition, the total power output, and the efficiency. The effects of composition, total mass flow rate, inlet pressure, and inlet temperature on the efficiency are examined.

## Analytical Model

### Governing Equations

A schematic of the CO laser system is shown in Fig. 1; the geometry is that of Ref. 1. Because of flow symmetry, the axial variation of the flow properties is assumed to be the same in each half of the tube. The model presented here treats molecules in different quantum states as different species. For such a mixture, the governing equations are the overall continuity, momentum and energy equations, the conservation of species equations, the equation of state, Ohm's law, and the

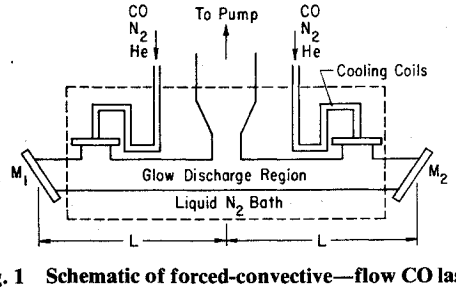


**Fig. 1 Schematic of forced-convective—flow CO laser.**

Presented as Paper 75-35 at the AIAA 13th Aerospace Sciences Meeting, Pasadena, Calif., Jan. 20-22, 1975; submitted Feb. 10, 1975; revision received July 14, 1975. Supported, in part, by NSF Grant GK-41610.

Index categories: Thermochemistry and Chemical Kinetics; Plasma Dynamics and MHD; Lasers.

*Visiting Assistant Professor of Mechanical and Aerospace Engineering. Member AIAA.

†Professor of Mechanical and Aerospace Engineering. Associate Fellow AIAA.

electron Boltzmann equation. For the steady one-dimensional approximation employed here, these equations take the form

$$\rho u A = \dot{m} \tag{1}$$

$$\rho u\, du/dx + dp/dx = 0 \tag{2}$$

$$\rho u\, (d/dx)\,[H + u^2/2] + jE - dq/dx \tag{3}$$

$$\rho u (d/dx)\; Y_s = m_s R_s \tag{4}$$

$$p = N_e k T_e + N k T \quad N = \sum_s N_s \quad s = \mathrm{CO, He, N_2} \tag{5}$$

$$j = e N_e \mu E \tag{6}$$

$$\frac{E^2}{3}\frac{d}{d\epsilon}\left[\frac{\epsilon}{\sum_s (N_s Q_{sm})}\frac{df}{d\epsilon}\right] + \sum_s\left[\frac{2m_e}{m_s}\frac{d}{d\epsilon}\left[\epsilon^2 N_s Q_{sm} f\right]\right] + \sum_s\left[\frac{2m_e}{m_s}\frac{kT}{e}\frac{d}{d\epsilon}\left[\epsilon^2 N_s Q_{sm}\frac{df}{d\epsilon}\right]\right] + \sum_s N_s\left[\sum_j (\epsilon+\epsilon_{sj}) f(\epsilon+\epsilon_{sj}) Q_{sj}(\epsilon+\epsilon_{sj}) - \epsilon f(\epsilon)\sum_j Q_{sj}(\epsilon)\right] = 0 \tag{7}$$

$$\mu = -\tfrac{1}{3}\frac{1}{(2e/m_e)^{1/2}}\int_0^\infty \frac{\epsilon (df/d\epsilon)}{\sum_s (N_s Q_{sm})}\, d\epsilon$$

$$T_e = \frac{2}{3}\left(\frac{e}{k}\right)\int_0^\infty \epsilon^{3/2} f(\epsilon)\, d\epsilon; \quad \int_0^\infty \epsilon^{1/2} f(\epsilon)\, d\epsilon = 1 \tag{8}$$

and $\rho$ is the density, $u$ is the mean velocity, $A$ is the area, $\dot{m}$ is the mass flow rate, $p$ is the pressure, $H$ is the specific enthalpy, $dq/dx$ is the sum of the spontaneous and stimulated emission losses, $j$ is the current density, $E$ is the electric field, $\mu$ is the electron mobility, $f$ is the electron distribution function, $\epsilon$ is the electron energy in electron volts, $k$ is Boltzmann's constant, $T$ is the temperature, $e$ is the electronic charge, and subscript $e$ denotes electrons. For any species $s$, $m$ is the particle mass, $R$ is the production rate, $N$ is the number density, $Y$ is the mass fraction, $Q_{sm}$ is the electron momentum transfer cross section, $Q_{sj}$ is the electron inelastic collision cross section, and $\epsilon_{sj}$ is the energy loss of the $j$th inelastic process.

The various kinetic processes considered in formulating expressions for the production rates $R_s$ are: 1) ionization of CO, 2) electron impact excitation of the first 8 vibrational levels of CO and $N_2$, 3) single quantum vibration-vibration ($V-V$) exchange collisions (CO-CO, CO-$N_2$, $N_2-N_2$), 4) single quantum vibration-translation ($V-T$) exchange collisions (CO$-$CO, CO$-$He, $N_2-$CO, CO$-N_2$, $N_2-$He, $N_2-N_2$), 5) spontaneous radiative decay by CO ($\Delta v = 1$ and $\Delta v = 2$), and 6) stimulated emission and absorption by CO. For the conditions under consideration, the production rate of the electrons is dominated by the ionization rate; thus,

$$R_e = K_I N_e N_{\mathrm{CO,O}} \tag{9}$$

where

$$K_I = \left(\frac{2e}{m_e}\right)^{1/2}\int_0^\infty \epsilon\, Q_{\mathrm{CO},I} f(\epsilon)\, d\epsilon \tag{10}$$

with $Q_{\mathrm{CO},I}$ being the CO ionization cross section. The expressions used for the $V-T$ and $V-V$ rate coefficients are given in the Appendix. All of the cross sections needed in Eq. (7), with the exception of the CO electronic excitation cross sections, are available in tabular form in Ref. 18. Cross sections for fourteen electronic excitation processes for CO are generated from semiempirical formulae given by Sawada et al.[19] Although the terms corresponding to inelastic collisions of the second kind were neglected in Eq. (7),[20] the rates for electron impact vibrational deexcitation from level $v$ to ground state are included in the production rates of the various excited states, and are computed from the cross sections $Q^*_{sv}$ for deexcitation. The $Q^*_{sv}$ are obtained from the $Q_{sv}$ by use of the principle of microscopic reversibility[21]:

$$\epsilon\, Q^*_{sv}(\epsilon) = (\epsilon + \epsilon_{sv})\; Q_{sv}(\epsilon + \epsilon_{sv}) \tag{11}$$

**Method of Solution**

When lasing is present in the system, the values of the intensities $I_{v,j}(x)$ are such that the average gain coefficient $\bar{\gamma}_{v,j}$ for each transition satisfies the threshold condition

$$\bar{\gamma}_{v,j} = \frac{1}{\ell}\int_0^\ell \gamma_{v,j}(x)\, dx = \alpha$$

$$\alpha = -\ln(r)/\ell \qquad r = (r_1 r_2)^{1/2} \tag{12}$$

where $\ell$ is the length of the active optical path, $r_1$ and $r_2$ are the mirror reflectivities, $\alpha$ is the threshold gain coefficient, and $J$ is the rotational quantum number that yields the maximum average gain coefficient for a given transition. The intensities $I_{v,j}(x)$ can be written as[22]

$$I_{v,J}(x) = I^+_{v,J}(0)\left[\exp\left[\int_0^x \gamma_{v,J}(\xi)\, d\xi\right] + \left(\frac{1}{r_1}\right)\exp\left[-\int_0^x \gamma_{v,j}(\xi)\, d\xi\right]\right] \tag{13}$$

where $I^+_{v,J}(0)$, the value of the component of the intensity in the positive $x$ direction at $x = 0$, is to be determined as part of the solution. If the various losses are such that the average gain coefficient for a particular transition is less than the threshold value, then the intensity for that transition is zero.

The expression for the gain coefficient[9] assumes that the rotational states are in equilibrium with the translational mode. Because of this assumption, it is not possible to predict the $J$ numbers that characterize the various lines that may contribute to the power output in a given vibrational band. Therefore, it is assumed that laser emission in a given band occurs on the $P$-branch exhibiting the maximum average gain. It is noted that the $J$ characterizing the maximum $P$-branch is not known a priori, but can be determined as part of the solution.

The present problem requires the solution of $2 + v^*_{\mathrm{CO}} + v^*_{\mathrm{N_2}}$ stiff first-order differential equations subject to the integral constraints indicated by Eq. (12) (values of $v^*_{\mathrm{CO}}$ and $v^*_{\mathrm{N_2}}$ as high as 45 and 35, respectively, were employed in this study). Thus, the governing system is no longer a differential system, but an integrodifferential system, which requires solution by an iterative scheme. The starting point for this iterative scheme is a solution of the Boltzmann equation [Eq. (7)] for a range of $E/N$ values (because axial variations dominate the flow, the discharge cannot be characterized by a single $E/N$) using a fourth-order Adams-Moulton predictor-corrector method. The resulting distribution function then is used to calculate the electron temperature and mobility and the various ionization and vibrational excitation rates that appear in the governing equations. A maximum average small signal gain calculation[17] is carried out next. The purpose of this calculation is to identify those bands whose maximum average small signal gain coefficient is greater or equal to the threshold value, and to determine the maximum $P$-branch transitions. This calculation then defines the subscripts $v$ and

**Table 1 Operating conditions and predicted lasing efficiencies**

| Case no. | $\dot{m}_{He}$ g/sec | $\dot{m}_{Co}$, g/sec | $\dot{m}_{N_2}$, g/sec | $\dot{m}$, g/sec | $P_{IN}$ Torr | $T_{IN}$, °K | $r$ | $J$ A | $P_{INPUT}$, kW | Efficiency, % |
|---|---|---|---|---|---|---|---|---|---|---|
| 1 | 1.480 | 0.392 | 0.168 | 2.04 | 27 | 110 | 0.806 | 0.105 | 2.0 | 25.1 |
| 2 | 1.480 | 0.392 | 0.168 | 2.04 | 27 | 125 | 0.806 | 0.113 | 2.0 | 18.7 |
| 3 | 1.676 | 0.196 | 0.168 | 2.04 | 27 | 110 | 0.806 | 0.122 | 2.0 | 18.7 |
| 4 | 1.648 | 0.392 | 0.0 | 2.04 | 27 | 110 | 0.806 | 0.126 | 2.0 | 22.1 |
| 5 | 1.480 | 0.560 | 0.0 | 2.04 | 27 | 110 | 0.806 | 0.109 | 2.0 | 23.9 |
| 6 | 0.824 | 0.196 | 0.0 | 1.02 | 27 | 110 | 0.806 | 0.151 | 2.0 | 18.8 |
| 7 | 1.648 | 0.392 | 0.0 | 2.04 | 54 | 110 | 0.806 | 0.094 | 2.0 | 17.5 |

$J$ characterizing the intensities of the various laser transitions. A set of nonzero values for $I^+_{v,J}(0)$ are assumed for these transitions, and the governing equations are integrated down the tube using an implicit numerical integration method designed to handle stiff differential equations.[23] From this calculation, the maximum average small signal gain coefficient is recalculated to determine if any adjustments need to be made in the vibrational bands considered or in their peak $P$ transitions. If such an adjustment is needed, or if Eq. (12) is not satisfied, then new sets of $I^+_{v,J}(0)$ are generated with a secant method. The process is repeated until convergence on $v$, $J$, and $I^+_{v,J}(0)$ is achieved. The $I^+_{v,J}(0)$ are considered converged when $\ln(\bar{\gamma}_{v,J}/\alpha) \leq 10^{-2}$ for all transitions. The laser power output is computed from the $I^+_{v,J}(0)$ as

$$P_{laser} = 2A\left[\frac{(1-r)}{r}\right]\sum_{v} I^+_{v,J}(0) \tag{14}$$

## Results and Discussion

The tube dimensions employed in this study correspond to those used in the experiment of Kan and Whitney.[1] The tube length is 100 cm and the diam is 2.5 cm. Because of the flow symmetry indicated in Fig. 1, the calculations are performed for only half of the tube over the distance $L = 50$ cm. The optical path length is $\ell = 2L$. Table 1 presents the operating conditions and predicted lasing efficiencies for the seven cases considered in this study.

The composition, total mass flow rate, inlet pressure, and input power used in cases 1 and 2 correspond to the operating conditions of Kan and Whitney's experiment. The current density is calculated from the given power input as

$$j = P_{input}/2A\int_0^L E(x)\,dx \tag{15}$$

with $E(0)$ chosen as 200 V/cm. Because the distribution of $E(x)$ is not known a priori, the calculation of $j$ for a given set of conditions is an iterative process. Their optical cavity was formed with a totally reflecting mirror and a 65% reflecting mirror; hence, the radiation field in their device is asymmetric. Because complete symmetry is assumed in this study, their cavity was approximated by choosing a reflectivity $r$, which gives the same threshold condition as the experiment, i.e., $r = (r_1 r_2)^{1/2}$. Cool[22] has shown that the ratio of minimum to maximum values of total intensity within the cavity is given by

$$I_{min}/I_{max} = 2\,(r_{min})^{1/2}/(1+r_{min}) \tag{16}$$

where $r_{min}$ is the smaller of the two reflectivities. For Kan and Whitney's experiment this ratio is 0.98, whereas it is 0.99 for our equivalent cavity. Hence, in both cases, the axial variation of the intensities is negligible and this is borne out by calculations. Furthermore, Rigrod[24] has shown that for a single-transition laser, the power output for an asymmetrical resonator is computed correctly from an equivalent symmetrical resonator if $r = (r_1 r_2)^{1/2}$ and the mirror losses are equal (in this analysis, the mirror losses are all assumed to be zero). Although his analysis cannot be applied directly to the multitransition case, it does suggest that the assumption of symmetry employed here is a good approximation.

Because the entrance temperature was not reported, calculations were performed for 100 and 125K (cases 1 and 2). Kan and Whitney measured an efficiency of 20% for 2.0 kW of input power. An efficiency of 18% is predicted for $T_{IN} = 125$ K, and an efficiency of 25.1% is predicted for $T_{IN} = 110$ K. A comparison of the calculated and measured relative intensities is presented in Table 2. Considering the uncertainty in the value of the inlet temperature, it is seen that the theory is in reasonable agreement with experiment.

Figure 2 presents a comparison of the evolution of the CO vibrational distribution with distance into the discharge cavity for both lasing and nonlasing conditions, whereas Fig. 3 presents a similar comparison of the axial variation of the gain coefficient of the 10→9 transition under the same conditions. The operating conditions are for case 4 of Table 1.

The nonlasing case is considered first. Referring to Figs. 2 and 3, it can be seen that initially only the first eight levels are significantly populated by electron impact vibrational excitation and $V-V$ anharmonic pumping, and the gain coefficient for 10→9 transition is negative. As the flow continues

**Table 2 Comparison of $J$ values and relative intensities of observed and calculated transitions**

| | Ref. 1 | | $T_{IN} = 110$°K | | $T_{IN} = 125$°K | |
|---|---|---|---|---|---|---|
| Vibrational band | Transitions | Relative intensity | Transitions | Relative intensity | Transitions | Relative intensity |
| 5→4 | P(12) | 0.1 | P(13) | 0.31 | | |
| 6→5 | P(12)-P(13) | 0.8 | P(13) | 1.0 | P(13) | 1.0 |
| 7→6 | P(11)-P(13) | 1.0 | P(12) | 0.774 | P(12) | 0.888 |
| 8→7 | P(12) | 0.5 | P(12) | 0.472 | P(12) | 0.619 |
| 9→8 | P(11)-P(12) | 0.4 | P(11) | 0.274 | P(12) | 0.381 |
| 10→9 | P(10)-P(12) | 0.2 | P(11) | 0.160 | P(12) | 0.226 |
| 11→10 | P(10)-P(11) | 0.2 | P(11) | 0.089 | P(11) | 0.131 |
| 12→11 | P(10) | 0.03 | P(10) | 0.049 | P(11) | 0.071 |
| 13→12 | P(9)-P(11) | 0.06 | P(10) | 0.025 | P(11) | 0.036 |
| 14→13 | P(9)-P(10) | 0.05 | P( 9) | 0.009 | P(11) | 0.011 |
| 15→14 | P(9) | 0.02 | P( 9) | $1.6\times10^{-5}$ | | |

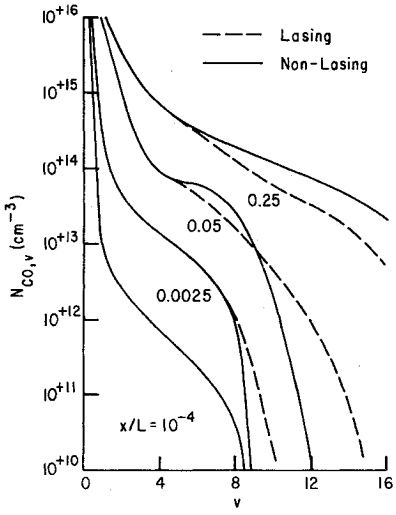


**Fig. 2 Effect of lasing on the CO vibrational distribution at selected distances into cavity.**

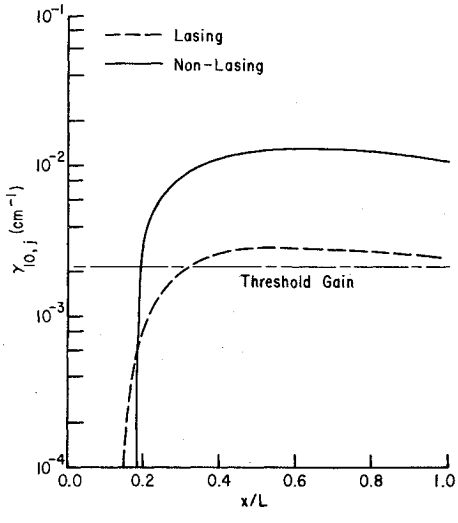


**Fig. 3 Effect of lasing on the axial variation of the gain coefficient for the 10→9 transition.**

into the cavity, the higher levels are populated by $V-V$ anharmonic pumping, and as the $V-V$ pumping continues to populate the upper levels, the gain for the 10→9 transition becomes positive and rises rapidly to its peak value. Beyond $x/L=0.35$, an essentially steady-state distribution is maintained, and the gain coefficient remains practically constant. The large value for the 10→9 transition gain coefficient is due to highly populated, almost level distribution produced among the intermediate levels.

The situation when lasing is present in the system is considered next. For the operating conditions of case 4, laser transitions occur on vibrational bands 5→4 to 14→13. Initially, only the first eight levels are significantly populated by electron impact excitation and $V-V$ pumping, and the gain coefficients for most of the lasing transitions are negative. Now when a beam of radiation with a frequency corresponding to a transition $v\rightarrow v-1$ passes through a region in which the gain coefficient for that transition is negative, molecules in the lower level $v-1$ will be pumped upward to the upper laser level $v$ by absorption of the radiation. Therefore, as the flow continues into the cavity, the upper levels are populated by two processes: $V-V$ anharmonic pumping and absorption of radiation. This effect is clearly visible in Fig. 2. At $x/L=2.5\times10^{-3}$, the populations of the first few levels above $v=8$ have been significantly increased by the absorption pumping mechanism. However, when the gain coefficient for a transition $v\rightarrow v-1$ becomes positive, the radiation will pump molecules downward from the upper level $v$ to the lower level $v-1$ by stimulated emission. This stimulated emission process opposes the $V-V$ anharmonic pumping process. Consequently, when the gain coefficient for a transition $v\rightarrow v-1$ becomes positive, the population of level $v$ in the lasing case drops below the corresponding value in the nonlasing case within a very small distance further downstream. Referring to Fig. 2, one can see that at $x/L=0.05$ the gain coefficients for transition 5→4 to 9→8 have become positive; hence, the stimulated emission process is responsible for maintaining the populations of levels 5-9 below their corresponding values in the nonlasing case. However, the gain coefficients for the higher transitions are still negative, and the absorption pumping mechanism continues to pump these upper levels above their corresponding values in the nonlasing case. Eventually, the gain coefficients for all of the lasing transitions become positive, and the stimulated emssion process maintains the populations of levels $v\leq5$ at values below those of the nonlasing case ($x/L=0.25$ and higher, see Fig. 2). Although the differences are too small to show in Fig. 2, once the gain coefficient for transition 5→4 becomes positive, the populations of levels $v\geq5$ at values below those of the nonlasing case become and remain greater than the corresponding values in the nonlasing case.

The influence of this absorption pumping/stimulated emission process can be seen in the behavior of the 10→9 transition gain coefficients depicted in Fig. 3. Because the absorption pumping process populates the upper levels faster than the $V-V$ pumping process does when lasing is absent, the 10→9 transition develops a positive gain coefficient at a smaller $x$ value in the lasing case. Once the gain coefficient become positive, stimulated emission opposes the $V-V$ pumping process and prevents the gain coefficient from attaining the larger value it had in the nonlasing case. In fact, the balance that is achieved between these two opposing processes in such that the resulting average gain coefficient is equal to the threshold value. Thus, one can see in Fig. 3 that the maximum value of the gain coefficient for the 10→9 transition is only slightly greater than the threshold value when lasing is allowed in the system. The maximum average small signal gain coefficient for the 5→4 transition is well below the threshold value when the entrance temperature is 125K, and is above the threshold value when the entrance temperature is 110K. Consequently, the 5→4 transition does not appear in the power calculation for case 2. However, the intensities for the higher transitions are independent of inlet temperature, even though substantial differences exist in the small signal gain coefficients, which increase with decreasing inlet temperature. This is a result of the absorption process discussed earlier. For the higher inlet temperatures, the gain coefficient remains negative for a greater distance into the cavity; therefore, the pumping resulting from the absorption process helps offset the decrease in the efficiency of the CO-CO $V-V$ pumping process.

Figure 4 shows the influence of the ratio of CO flow rate to that of He on intensity. The CO flow rate is reduced by a factor of two, and the He flow rate is increased to maintain a constant total mass flow rate of 2.04 g/sec. All other operating parameters remain the same. It is seen that the intensity on the 5→4 transition increases with a decrease in the CO flow rate, whereas all of the other intensities decrease. Since the total number of CO molecules has been reduced, the net $V-V$ pumping rate is reduced, and it takes longer to excite a given number of molecules to an upper level. Thus, for the same transit time in the discharge region, the lower $V-V$ pumping rate will have time only to significantly populate the lower levels. This result indicates that the lower level transitions can be obtained by reducing the CO concentration. However, these lower transitions are obtained at the expense of reduced efficiency.

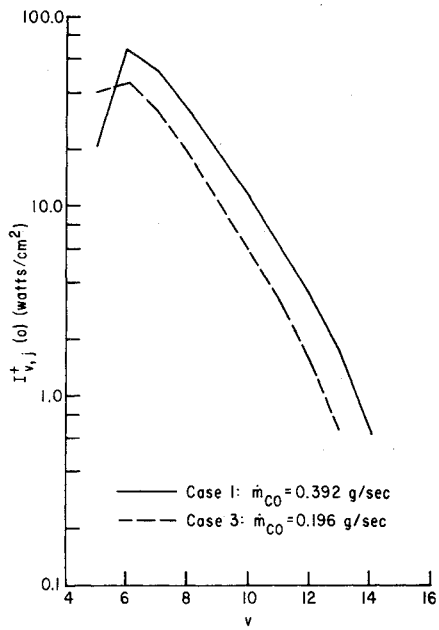


**Fig. 4 Influence of CO-He flow rate ratio on the lasing intensities.**

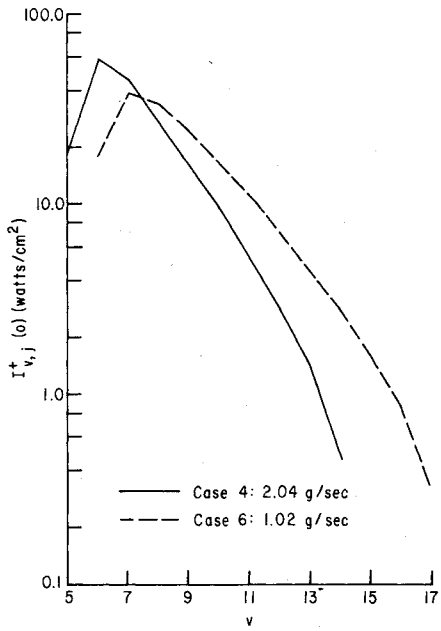


**Fig. 5 Influence of total mass flow rate on the lasing intensities.**

The influence of $N_2-He$ and $N_2-CO$ flow rate ratios on intensity are considered next. When the $N_2$ flow rate was replaced by He (case 4), a small decrease in the intensities was observed. This is because replacing $N_2$ with He is equivalent to removing a source of vibrational energy for CO. On the other hand, when $N_2$ is replaced by CO, all of the energy expended in exciting $N_2$ is now available to excite CO. For case 5, this gave a 7% increase in the vibrational excitation of CO, resulting in a slight increase in the intensities for the transitions $v \geq 6$. However, since the CO mass flow rate has been increased with a resulting increase in the net CO $V-V$ pumping rate, more molecules will be pumped into the upper levels at the expense of molecules in the lower levels. This effect led to the loss of the $5 \rightarrow 4$ transition for case 5, and hence a reduction in efficiency as compared to case 1.

The influence of the total mass flow rate on the intensity is shown in Fig. 5. The total mass flow rate is reduced by a factor of two. Because the inlet pressure and temperature were not changed, this amounts to decreasing the inlet velocity by a factor of two, and thus increasing the transit time in the discharge region. The behavior indicated in Fig. 5 may be traced to two competing effects: when the transit time is increased, the effectiveness of the convective cooling is reduced, and this results in an increased gas temperature. For case 4, the exit gas temperature is 152K, whereas for case 6 it is 232K. On the other hand, the increased transit time results in more molecules being pumped to higher levels by $V-V$ pumping and by the radiation absorption mechanism discussed previously. The net effect is a general shift to the higher vibrational levels.

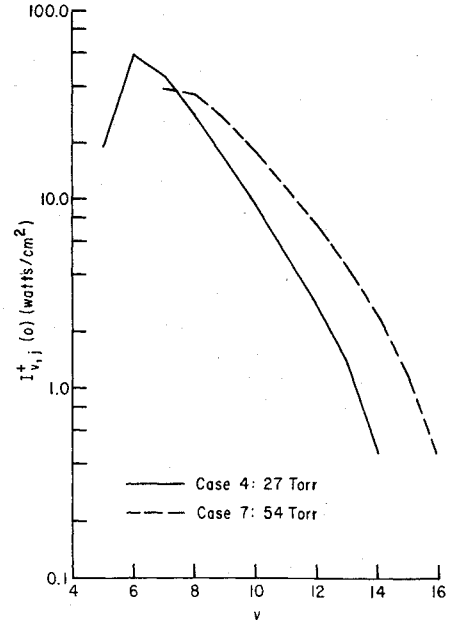


**Fig. 6 Influence of inlet pressure on the lasing intensities.**

Figure 6 presents the influence of the inlet pressure. The inlet pressure is doubled, but the relative proportions of CO and He remain the same. Because the inlet temperature remains the same, doubling the inlet pressure doubles the gas density, and this results in halving the velocity in order to maintain the same total flow rate. Therefore, increasing the inlet pressure produces the same effect as reducing the total mass flow rate. Hence, the behavior of the intensities in Fig. 6 is the same as that in Fig. 5. However, there is an additional factor to consider. Since an increase in $p$ produces an increase in $N$, and thus a reduction in $E/N$, the average $T_e$ for case 7 is lower than the average $T_e$ for case 6. Consequently, the electron pumping rates in case 7 are lower than those in case 6, resulting in the loss of both the $6 \rightarrow 5$ and $5 \rightarrow 4$ transitions in case 7 as opposed to just the loss of the $5 \rightarrow 4$ transition in case 6.

## Conclusions

As a result of this study, a new effect, which does not appear in transverse flow lasers, has been identified. When lasing is present in the system the upper levels, in the entrance region in which the gain coefficients are negative are pumped above their corresponding values in the nonlasing case as a result of radiation absorption. This effect has the tendency to make the intensities of the higher levels ($v > 8$) less sensitive to changes in the gas temperature and residence time.

For a given input power and $N_2$ fraction, the results indicate that the three most influential operating parameters are the temperature, velocity, and CO fraction. The efficiency is increased by reducing the temperature, increasing the flow velocity, and/or increasing the fraction of CO in the system. However, transitions on the lower vibrational bands can be obtained at the expense of efficiency by reducing the CO fraction. A slight reduction in efficiency occurs if the $N_2$ in the system is replaced with either CO or He.

Finally, for a given velocity, the correlation between the effect of a parameter on the maximum average small signal gain coefficients and its effect on the intensities of the lasing transitions is quite good, thereby demonstrating the value of the less expensive small signal gain calculations for analyzing new laser systems.

## Appendix: $V-T$ and $V-V$ Rate Coefficients

The $V-T$ rate model employed here is based on a modified Schwartz-Slawsky-Herzfeld (SSH) theory.[25] The first two modifications are due to Keck and Carrier.[26] In the first modification, the vibrating molecule was treated as a Morse oscillator rather than a harmonic oscillator. Because the SSH theory is valid in the adiabatic limit, the second modification consisted of employing an adiabacity factor to bridge the gap between impulsive and adiabatic energy exchanges. Bray[27] first introduced this modified SSH theory in analytical studies of vibrational relaxation and his particular formulation has been widely used in many theoretical studies of CO lasers. The third modification employed here is due to Shin.[28] Simple SSH theory assumes an exponential repulsive interaction potential between the colliding molecules. In an actual case, the potential between two molecules includes an attractive well, and this can affect the transition probabilities at low temperatures. Shin showed that use of a Morse potential, which has an attractive well and which adequately approximates true intermolecular potentials, provides a multiplicative factor to the SSH theory and improves the predictions of theory at low temperatures. Based on these considerations, the $V-T$ rate coefficients may be written as

$$VT_v^{st} = K_{VT}^{st}\, T\, Z_{st}\, \frac{v}{(1-v\delta_s)} \exp\left[\frac{\theta_v^s}{2T}\right] F(y_v^{st})$$

$$\times \exp\left[\frac{4}{\pi (T_{st}^*)^{1/2}} (y_v^{st})^{1/3} + \frac{16}{3\pi^2 T_{st}^*}\right] \tag{A1}$$

where

$$\theta_v^s = (E_v^s - E_{v-1}^s)/k \qquad y_v^{st} = [b_{st}(\theta_v^s)^2/8T]^{1/2}$$

$$b_{st} = 16\,\pi^4 k\,\mu_{st}\ell_{st}/h^2 \qquad \delta_s = (\omega_e x_e/\omega_e)_s$$

$$\mu_{st} = m_s m_t/(m_s+m_t) \qquad T_{st}^* = T/\epsilon_{st} \tag{A2}$$

$h$ is Planck's constant and $E_v^s$ is the vibrational energy of the $v$th vibrational levels of species $s$. The vibrational constants $\omega_e$ and $\omega_e x_e$ for CO and $N_2$ are obtained from Refs. 29 and 30. The adiabaticity factor $F(y)$ is obtained from

$$F(y) = \tfrac{1}{2} \exp(-2y/3)[3-\exp(-2y/3)] \tag{A3}$$

for $0 \le y \le 21.622$ and from

$$F(y) = 8\,(\pi/3)^{1/2} y^{7/3} \exp(-3y^{2/3}) \tag{A4}$$

for $y > 21.622$. Equation (A3) is Keck and Carrier's[26] empirical fit and Eq. (A4) is from the original SSH theory.[25]

Examination of the expression resulting from the previous modifications to the SSH theory indicates that it has a minimum at some low temperature $T_c^{st}$. On the other hand, low temperature measurements[31] of the $V-T$ rate coefficient for CO deactivation by He and $H_2$ are constant below a certain temperature when expressed in $\sec^{-1}\,\mathrm{Torr}^{-1}$. Therefore $VT_v^{st}$ (in units of $\sec^{-1}\,\mathrm{Torr}^{-1}$) is assumed constant for $T < T_c^{st}$. The constants $K_{VT}^{st}$, $\ell_{st}$, and $T_c^{st}$ were determined from a least-squares fit of available measurements,[31-38] and are listed in Table A1. The well depth $\epsilon_{st}$ and are listed in Table A1. The well depth $\epsilon_{st}$ and collision frequency $Z_{st}$ are obtained from Eqs. (A10) and (A11).

**Table A1 Empirical constants for $V-T$ rate coefficients**

| | $K_{VT}^{st}$, °K$^{-1}$ | $\ell_{st}$, Å | $T_c^{st}$, °K |
|---|---|---|---|
| CO–CO | $4.5\times10^{-5}$ | 0.203 | 135 |
| CO–He | $7.15\times10^{-5}$ | 0.297 | 152 |
| $N_2$–$N_2$ | $2.86\times10^{-5}$ | 0.203 | 134 |
| $N_2$–He | $1.55\times10^{-5}$ | 0.317 | 145 |

No experimental data are available for the rates for CO deactivation by $N_2$ and $N_2$ deactivation by CO. However, because CO and $N_2$ have the same mass, simple SSH theory predicts that

$$VT_v^{CO-N_2} = VT_v^{CO-CO}$$

$$VT_v^{N_2-CO} = VT_v^{N_2-N_2} \tag{A5}$$

and this was assumed here.

The $V-V$ transition probability is high if the resonance defect is small and small if the resonant defect is high. Small-resonance-defect $V-V$ transitions are dominated by the long-range part of the intermolecular potential created by the multipole forces.[39-41] When the resonance defect is large, the $V-V$ transition probabilities are determined by the short-range repulsive core of the intermolecular potential via a process similar to $V-T$ relaxation. Consequently, it was proposed[40,41] that $V-V$ transition probabilities be treated as the sum of two contributions, one from a long-range multipole interaction and the other from a short-range repulsive force interaction. This theory was applied to CO–CO $V-V$ transitions and was found to be in good agreement with experiment.[42]

The $V-V$ rate model used in this study is based on a simplified version of Jeffers and Kelley's theory.[40] The simple formulation is due to Rockwood et al.[5]; in this formulation, the long-range portion is approximated by a simple Gaussian function of the resonance defect, whereas the short-range portion is given by the modified SSH theory. The resulting expressions for the $V-V$ rate coefficients are written as

$$VV_{v,v'}^{st} = L_{v,v'}^{st} + S_{v,v'}^{st} \tag{A6}$$

where

$$L_{v,v'}^{st} = A_{st}\frac{Z_{st}}{T}\left|\frac{R_{v,v-1}^s}{R_{1,0}^s}\right|^2\left|\frac{R_{v'+1,v'}^t}{R_{1,0}^t}\right|^2$$

$$\times \exp\left[\frac{\theta_{v,v'}^{st}}{2T}\right] \exp\left[-\frac{(\theta_{v,v'}^{st})^2}{W_{st}T}\right] \tag{A7}$$

$$S_{v,v'}^{st} = K_{VV}^{st}\, T\, Z_{st}\, \frac{v}{(1-v\delta_s)}\, \frac{(v'+1)}{[1-(v'+1)\delta_t]}$$

$$\times \exp\left[\frac{\theta_{v,v'}^{st}}{2T}\right] F(y_{v,v'}^{st})$$

$$\times \exp\left[\frac{4}{\pi (T_{st}^*)^{1/2}} (y_{v,v'}^{st})^{1/3} + \frac{16}{3\pi^2 T_{st}^*}\right] \tag{A8}$$

and

$$\theta_{v,v'}^{st} = (E_v^s - E_{v-1}^s - E_{v'+1}^t + E_{v'}^t)/k$$

$$y_{v,v'}^{st} = \left[\frac{b_{st}(\theta_{v,v'}^{st})^2}{8T}\right]^{1/2} \tag{A9}$$

$b_{st}$, $\delta_s$, $\delta_t$, $T_{st}^*$, and $F(y)$ are obtained from Eqs. (A2-A4). The quantity $|R_{v,v-1}^s/R_{1,0}^s|^2$ is the vibrational matrix element of the dominant electric multipole moment of molecule $s$. For CO the dipole moment is dominant, and the corresponding dipole matrix elements are taken from Young and

**Table A2 Empirical constants for $V-V$ rate coefficients**

| | $A_{st}$, °K | $W_{st}$, | $K^{s,t}_{VV}$, °K$^{-1}$ | $\ell_{st}$, Å |
|---|---|---|---|---|
| CO−CO | 1.17 | 64.2 | $3.06\times10^{-7}$ | 0.203 |
| CO−$N_2$ | 1.42 | 47.7 | $6.95\times10^{-8}$ | 0.203 |
| $N_2-N_2$ | ... | ... | $3.06\times10^{-7}$ | 0.203 |

Eachus,[43] whereas for $N_2$ the electric quadrupole moment is dominant, and the corresponding quadrupole matrix elements are computed from the expression given by Heaps and Herzberg[44] for a linear quadrupole moment with a Morse oscillator. The constants $A_{st}$, $W_{st}$, and $K^{s,t}_{VV}$ were determined from a least-squares fit of available data[36,42,45-52] and are given in Table 2A. The values of $\ell_{CO\text{-}CO}$ and $\ell_{N_2N_2}$ were taken from the $V-T$ rate expressions, and $\ell_{CO\text{-}N_2}$ is estimated from $\ell_{CO\text{-}N_2}=(\ell_{CO\text{-}CO}\ \ell_{N_2\text{-}N_2})^{1/2}$. No experimental data are available for $N_2$-$N_2$ $V-V$ transitions, but simple SSH theory predicts that $K_{VV}{}^{CO\text{-}Co}=K_{VV}{}^{N_2\text{-}N_2}$, and this is assumed here.

The collision frequencies $Z_{st}$ that appear in the $V-T$ and $V-V$ rate coefficients are calculated from the Lennard-Jones potential parameters of the colliding molecules[53]

$$Z_{st}=d^2_{st}\Omega^{(2,2)}(T^*_{st})\,(8\pi\ k\ T/\mu_{st})^{1/2} \tag{A10}$$

where

$$d_{st}=(d_s\ d_t)^{1/2}$$

$$\epsilon_{st}=2(\epsilon_s\ \epsilon_t I_s\ I_t)^{1/2}/(I_s+I_t) \tag{A11}$$

$T^*_{st}$ and $\mu_{st}$ are defined in Eq. (A2), the combining rules given in Eq. (A11) are from Good and Hope,[54,55] $\Omega^{(2,2)}(T)$ is obtained from an empirical curve fit,[56] $\epsilon_s$ and $d_s$ are obtained from Ref. 53, and $I_s$ is the ionization potential for species $s$.

## References


[1] Kan, T. and Whitney, W., "Forced-Convective-Flow Carbon Monoxide Laser," *Applied Physics Letters*, Vol. 21, Sept. 1972, pp. 213-215.

[2] Jeffers, W. Q. and Wiswall, C. E., "Analysis of Pulsed CO Lasers," *Journal of Applied Physics*, Vol. 42, Nov. 1971, pp. 5059-5065.

[3] Abraham, G. and Fisher, E. R., "Modeling of a Pulsed CO/$N_2$ Molecular Laser System," *Journal of Applied Physics*, Vol. 43, Nov. 1972, pp. 4621-4631.

[4] Fisher, E. R., "Modeling of a Pulsed CO/$N_2$ Molecular Laser System. II. Effect of Mixture Components and Temperature Variation," *Journal of Applied Physics*, Vol. 44, Nov. 1973, pp. 5031-5034.

[5] Rockwood, S. D., Brau, J. E., Proctor, W. A., and Canavan, G. H., "Time-Dependent Calculations of Carbon Monoxide Laser Kinetics," *IEEE Journal of Quantum Electronics*, Vol. QE-9, Jan. 1973, pp. 120-129.

[6] Lacina, W. B., Mann, M. M., and McAllister, G. L., "Transient Oscillator Analysis of a High-Pressure Electrically Excited CO Laser," *IEEE Journal of Quantum Electronics*, Vol. QE-9, June 1973, pp. 588-593.

[7] Rich, J. W., "Kinetic Modeling of the High-Power Carbon Monoxide Laser," *Journal of Applied Physics*, Vol. 42, June 1971, pp. 2719-2730.

[8] Center, R. E. and Caledonia, G. E., "Theoretical Description of the Electrical CO Laser," *Applied Physics Letters*, Vol. 19, Oct. 1971, pp. 211-213.

[9] Lacina, W. B., "Kinetic Model and Theoretical Calculations for Steady State Analysis of Electrically Excited CO Laser Amplifier System-Final Report: Part II," Northrop Corporation Laboratories, Hawthorne, Calif., NCL 71-32R, Aug. 1971.

[10] Rich, J. W., Lordi, J. A., and Kang, S. W., "Semi-Annual Technical Report, Supersonic Electrically Excited Laser Development," Calspan Corp., Buffalo, N.Y., WG-5164-A-1, Dec. 1972.

[11] Rich, J. W., Bergman, R. C., and Lordi, J. A., "Experimental and Theoretical Investigation of the Electrically Excited, Supersonic Flow Carbon Monoxide Laser," AIAA Paper 74-179, presented at AIAA 12th Aerospace Sciences Meeting, Washington, D. C., Jan. 30-Feb. 1, 1974.

[12] Rich, J. W., Lordi, J. A. Gibson, R. A., and Kang, S. W., "Final Technical Report, Supersonic Electrically Excited Laser Development," Calspan Corp., Buffalo, N. Y., WG-5164-A-3, Mar. 1974.

[13] Plummer, M. J. and Glowacki, W. J., "Theoretical Investigation of the CO Supersonic Electric Discharge Laser," AIAA Paper 73-623, presented at AIAA 6th Fluid and Plasma Dynamics Conference, Palm Springs, Calif., July 16-18, 1973.

[14] Lordi, J. A., Falk, T. J., and Rich, J. W., "Analytical Studies of the Kinetics of Electrically Excited, Continuously Operating CO Flow Lasers," AIAA Paper 74-563, presented at AIAA 7th Fluid and Plasma Dynamics Conference, Palo Alto, Calif., June 17-19, 1974.

[15] Hall, R. J. and Eckbreth, A. C., "Kinetic Modeling of CW CO Electric-Discharge Lasers," *IEEE Journal of Quantum Electronics*, Vol. QE-10, Aug. 1974, pp. 580-590.

[16] Smith, N. S., Hassan, H. A., and McInville, R. M., "Analysis of High-Flow Electric Discharge CO Laser Systems," AIAA Paper 74-180, presented at AIAA 12th Aerospace Sciences Meeting, Washington, D.C., Jan. 30-Feb. 1, 1974.

[17] Smith N. S., Hassan, H. A., and McInville, R. M., "Small Signal Gain Calculations for High Flow CO Discharge Lasers," *AIAA Journal*, Vol. 12, Dec. 1974, pp. 1619-1620.

[18] Kieffer, L. J., "A Compilation of Electron Collision Cross Section Data for Modeling Gas Discharge Lasers," Information Center, Joint Institute for Laboratory Astrophysics, University of Colorado, Boulder, Colorado, JILA Rept. 13, Sept. 1973.

[19] Sawada, T., Sellin, D. L., and Green, A. E. S., "Electron Impact Excitation Cross Sections and Energy Degradation in CO," *Journal of Geophysical Research*, Vol. 77, Sept. 1972, pp. 4819-4828.

[20] Frost, L. S. and Phelps, A. V., "Rotational Excitation and Momentum Transfer Cross Sections for Electrons in $H_2$ and $N_2$ from Transport Coefficients," *Physical Review*, Vol. 127, Sept. 1962, pp. 1621-1633.

[21] Ross, J., Light, J. C., and Schuler, K. E., "Rate Coefficients, Reaction Cross Sections, and Microscopic Reversibility," *Kinetic Processes in Gases and Plasma*, 1st ed., Academic Press, N. Y., 1969, pp. 281-320.

[22] Cool, T. A., "Power and Gain Characteristics of High Speed Flow Lasers," *Journal of Applied Physics*, Vol. 40, Aug. 1969, pp. 3565-3573.

[23] Gear, C. W., "The Automatic Integration of Ordinary Differential Equations," *Communications of the ACM*, Vol. 14, Mar. 1971, pp. 176-179.

[24] Rigrod, W. W., "Saturation Effects in High-Gain Lasers," *Journal of Applied Physics*, Vol. 36, Aug. 1965, pp. 2487-2490.

[25] Herzfeld, K. F. and Litovitz, T. A., Absorption and Dispersion of Ultrasonic Waves, 1st. ed., Academic Press, N.Y., 1959, pp. 260-350.

[26] Keck, J. and Carrier, G., "Diffusion Theory of Nonequilibrium Dissociation and Recombination," *Journal of Chemical Physics*, Vol. 43, Oct. 1965, pp. 2284-2298.

[27] Bray, K. N. C., "Vibrational Relaxation of Anharmonic Oscillator Molecules: Relaxation Under Isothermal Conditions," *Journal of Physics B*, Vol. 1, Ser. 2, Aug. 1968, pp. 705-717.

[28] Shin, H. K., "Dependence of the Probabilities of Vibrational De-Excitation on Interaction Potentials," *The Journal of Chemical Physics*, Vol. 42, Jan. 1965, pp. 59-62.

[29] Patel, C. K. N., "CW Laser on Vibrational-Rotational Transition of CO," *Applied Physics Letters*, Vol. 7, Nov. 1965, pp. 246-247.

[30] Herzberg, G., *Molecular Spectra and Molecular Structure I. Spectra of Diatomic Molecules*, 2nd ed., Van Nostrand Reinhold, New York, 1950, pp. 552-553.

[31] Miller, D. J. and Millikan, R. C., "Vibrational Relaxation of Carbon Monoxide by Hydrogen and Helium down to 100°K," *The Journal of Chemical Physics*, Vol. 53, Oct. 1970, pp. 3384-3385.

[32] Hooker, W. J. and Millikan, R. C., "Shock-Tube Study of Vibrational Relaxation in Carbon Monoxide for the Fundamental and First Overtone," *The Journal of Chemical Physics*, Vol. 38, Jan. 1963, pp. 214-220.

[33] Kovacs, M. A., "VT Relaxation in $N_2$ and CO," *IEEE Journal of Quantum Electronics*, Vol. QE-9, Jan. 1973, p. 189.

[34] Millikan, R. C., "Carbon Monoxide Vibrational Relaxation in Mixtures with Helium, Neon, and Krypton," *The Journal of Chemical Physics*, Vol. 40, May 1964, pp. 2594-2596.

[35] Millikan, R. C., "Vibrational Fluorescence of Carbon Monoxide," *The Journal of Chemical Physics*, Vol. 38, June 1963, pp. 2855-2860.

[36]Green, W. H. and Hancock, J. K., "Measurement of CO ($v=1$) Vibrational Energy Transfer Rates Using a Frequency-Doubled $CO_2$ Laser," *The Journal of Chemical Physics*, Vol. 59, Oct. 1973, pp. 4326-4335.

[37]Millikan, R. C. and White, D. R., "Vibrational Energy Exchange Between $N_2$ and CO. The Vibrational Relaxation of Nitrogen," *The Journal of Chemical Physics*, Vol. 39, July 1963, pp. 98-101.

[38]White, D. R., "Vibrational Relaxation of Shocked $N_2$-He, $N_2$-$CH_4$, and $N_2$-$C_2$-$H_2$ Mixtures," *The Journal of Chemical Physics*, Vol. 55, Nov. 1971, pp. 4433-4437.

[39]Sharma, R. D. and Brau, C. A., "Energy Transfer in Near-Resonant Molecular Collisions due to Long-Range Forces with Application to Transfer of Vibrational Energy from $\nu_3$ Mode of $CO_2$ to $N_2$," *The Journal of Chemical Physics*, Vol. 53, Jan. 1969, pp. 924-930.

[40]Jeffers, W. Q. and Kelley, J. D., "Calculations of $V-V$ Transfer Probabilities in CO-CO collisions," *The Journal of Chemical Physics*, Vol. 55, Nov. 1971, pp. 4433-4437.

[41]Caledonia, G. E. and Center, R. E., "Vibrational Distribution Functions in Anharmonic Oscillators," *The Journal of Chemical Physics*, Vol. 55, July 1971, pp. 552-561.

[42]Hancock, G. and Smith, I. W. M., "Quenching of Infrared Chemiluminescene. 1: The Rates of De-Excitation of CO ($4<v<13$) by He, Co, NO, $N_2$, $O_2$, OCS, $N_2O$, and $CO_2$," *Applied Optics*, Vol. 10, Aug. 1971, pp. 1827-1842.

[43]Young, L. A. and Eachus, W. J., "Dipole Moment Function and Vibration-Rotation Matrix Elements for CO," *The Journal of Chemical Physics*, Vol. 44, June 1966, pp. 4195-4206.

[44]Heaps, H. S. and Herzberg, G., "Intensity Distribution in the Rotation-Vibration Spectrum of the OH Molecule," *Zeitschrift Fur Physik*, Vol. 133, Sept. 1952, pp. 48-64.

[45]Jeffers, W. Q. and Powell, H. T., "Carbon Monosulfide and CO Probe Laser Research," Radiation Sciences Dept., McDonnell MDC Q0498, July 1973, Douglas Research Laboratories, McDonnell Douglas Corp., St. Louis, Mo..

[46]Powell, H. T., "Vibrational Relaxation of Carbon Monoxide Using a Pulsed Discharge," *The Journal of Chemical Physics*, Vol. 59, Nov. 1973, pp. 4937-4941.

[47]Powell, H. T., private communication.

[48]Stephenson, J. C., "Vibrational Excitation and Relaxation of the CO ($v=1$) and CO ($v$-2) States," *Applied Physics Letters*, Vol. 22, June 1973, pp. 576-578.

[49]Stephenson, J. C. and Mosburg, E. R., Jr., "Vibrational Energy Transfer in CO from 100 to 300 K," *The Journal of Chemical Physics*, Vol. 60, May 1974, pp. 3562-3566.

[50]Zittel, P. F. and Moore, C. B., "Vibration-to-Vibration Energy Transfer in $N_2$-CO," *Applied Physics Letters*, Vol. 21, Aug. 1972, pp. 81-82.

[51]Sato, Y., Tsuchiya, S., and Kuratani, K., "Shock-Wave Study of Vibrational Energy Exchange between Diatomic Molecules," *The Journal of Chemical Physics*, Vol. 50, Mar. 1969, pp. 1911-1919.

[52]von Rosenberg, C. W., Jr., Bray, K. N. C., and Pratt, N. H., "Shock Tube Vibrational Relaxation Measurements: $N_2$ Relaxation by $H_2O$ and the CO-$N_2$ $V-V$ Rate," *The Journal of Chemical Physics*, Vol. 56, Apr. 1972, pp. 3230-3237.

[53]Hirschfelder, J. O., Curtiss, C. F., and Bird, R. B., *Molecular Theory of Gases and Liquids*, 2nd ed., Wiley, New York, 1964, pp. 1110-1111.

[54]Good, R. J. and Hope, C. J., "New Combining Rule for Intermolecular Distances in Intermolecular Potential Functions," *The Journal of Chemical Physics*, Vol. 53, July 1970, pp. 540-543.

[55]Good, R. J. and Hope, C. J., "Test of Combining Rules for Intermolecular Distances. Potential Function Constants from Section Virial Coefficients," *The Journal of Chemical Physics*, Vol. 55, July 1971, pp. 11-116.

[56]Neufeld, P. D., Janzen, A. R., and Arziz, R. A., "Empirical Equations to Calculate 16 of the Transport Collision Integrals $\Omega^{(l,s)*}$ for the Lennard-Jones (12-6) Potential," *The Journal of Chemical Physics*, Vol. 57, Aug. 1972, pp. 1100-1102.